# Visual MRI: Merging Information Visualization and non-parametric clustering techniques for MRI data set analysis

Umberto Castellani [a,*] Marco Cristani [a] Carlo Combi [a]

Vittorio Murino [a] Andrea Sbarbati [b] Pasquina Marzola [b]

[a] *Dipartimento di Informatica, Università degli Studi di Verona*

*Ca' Vignal 2, Strada Le Grazie 15*

*37134 Verona, Italia*

*e-mail: {umberto.castellani,marco.cristani,carlo.combi,vittorio.murino}@univr.it*

[b] *Dipartimento di Scienze Morfologiche Biomediche, Università degli Studi di Verona*

*P.le Scuro, 10, Policlinico B.go Roma*

*37134 Verona, Italia*

*e-mail: {andrea.sbarbati,pasquina.marzola}@univr.it*

---

**Summary**

***Objective.*** This paper presents *Visual MRI*, an innovative tool for the magnetic resonance imaging (MRI) analysis of tumoral tissues. The main goal of the analysis is to separate each magnetic resonance image in meaningful clusters, highlighting zones which are more probably related with the cancer evolution. Such non-invasive analysis serves to address novel cancer treatments, resulting in a less destabilizing and more effective type of therapy than the chemotherapy-based ones. The advancements brought by *Visual MRI* are two: first, it is an integration of effective infor-

mation visualization (IV) techniques into a clustering framework, which separates each MRI image in a set of informative clusters; the second improvement relies in the clustering framework itself, which is derived from a recently re-discovered non-parametric grouping strategy, i.e., the *mean shift*.

***Methodology.*** The proposed methodology merges visualization methods and data mining techniques, providing a computational framework that allows the physician to move effectively from the MRI image to the images displaying the derived parameter space. An unsupervised non-parametric clustering algorithm, derived from the *mean shift* paradigm, and called *MRI-mean shift*, is the novel data mining technique proposed here. The main underlying idea of such approach is that the parameter space is regarded as an empirical probability density function to estimate: the possible separate modes and their attraction basins represent separated clusters. The mean shift algorithm needs sensibility threshold values to being set, which could lead to highly different segmentation results. Usually, these values are set by hands. Here, with the *MRI-mean shift* algorithm, we propose a strategy based on a structured optimality criterion which faces effectively this issue, resulting in a completely unsupervised clustering framework. A *Linked Brushing* visualization technique is then used for representing clusters on the parameter space *and* on the MRI image, where physicians can observe further anatomical details. In order to allow the physician to easily use all the analysis and visualization tools, a visual interface has been designed and implemented, resulting in a computational framework susceptible of evaluation and testing by physicians.

***Results.*** *Visual MRI* has been adopted by physicians in a real clinical research setting. To describe the main features of the system, some examples of usage on real cases are shown, following step by step all the actions scientists can do on an MRI image. To assess the contribution of *Visual MRI* given to the research setting, a validation of the clustering results in a medical sense has been carried out.

***Conclusions.*** From a general point of view, the two main objectives reached in this paper are: 1) merging information visualization and data mining approaches to support clinical research, 2) proposing an effective and fully automated clustering technique. More particularly, a new application for MRI data analysis, named *Visual MRI*, is proposed, aiming at improving the support of medical researchers in the context of cancer therapy; moreover, a non parametric technique for cluster analysis, named *MRI-mean shift*, has been drawn. The results show the effectiveness and the efficacy of the proposed application.

*Key words:* Information Visualization, Non-parametric Clustering, Magnetic Resonance Imaging, Mean Shift, Linked Brushing, Visual Mining, Dynamic Contrast Enhancement Magnetic Resonance Imaging (DCE-MRI), Cancer Therapy.

---

## 1 Introduction

The research interest on visualization and analysis of multidimensional data has grown rapidly during the last decade [1–4]. Focusing on medical applications, several activities require the visual investigation and analysis of images, video, and graphs [5, 6]. For this reason, *human computer interaction* and *information visualization* (IV) [3] methodologies have been proven to be very useful in supporting physicians in decision-based activities, such as those related to diagnoses and therapies. Furthermore, when dealing with a huge amount of data, automatic techniques for the reduction and simplification of the given data set as well as for the recognition of relevant patterns are needed: several kinds of *data mining* (DM) techniques have been proposed to deal with

* Corresponding author: tel. +39-045-8027988, fax +39-045-8027068

this issue, even in medical domains [7, 8].

Even though IV and DM are often considered two distinct research areas, their components could have complementary and synergic roles inside the same application, as highlighted in [6]. Indeed, from one side, effective interaction paradigms could allow the user to detect what would pass unnoticed through automatic systems: this research direction has been called Visual Data Mining [9] and has been considered even in the medical domain, as for example in [10]. On the other side, the proper visual representation of what has been discovered by data mining techniques could allow physicians to have a more accurate and exhaustive comprehension of the considered clinical problem.

Although several examples of either visualization [11–15] or analysis of medical images [16–18] have been proposed in literature, at the best of our knowledge, few work concerned with the integration of these two approaches.

With respect to this scenario, in this paper we specifically aim at integrating the use of IV techniques and clustering algorithms for the analysis of MRI data sets. The proposed work has been developed in the context of cancer research and, specifically, in testing antiangiogenic drugs. Differently from traditional therapies, antiangiogenic drugs are not directed against tumor cells, but against tumor vasculature. Preclinical and clinical evaluation of the efficacy of antiangiogenic compounds arises new problems to researchers because the traditional criterion for assessing the response of a tumor to a treatment, based on the measurement of tumor size reduction, is no longer valid [19]. Actually, the antiangiogenic efficacy is not necessarily accompanied by the tumor size regression. For this reason, testing of antiangiogenic compounds requires imaging methods that can detect vascular alteration. Dynamic Con-

trast Enhanced MRI (DCE-MRI) techniques play a relevant role in this field [19, 20]. DCE-MRI with macromolecular contrast agents has been used to measure characteristics of tumor microvessels such as transendothelial permeability ($k$PS) and fractional plasma volume ($f$PV) that are accepted surrogate markers of tumor angiogenesis [19].

In order to improve the analysis of such kind of data, an efficient and effective visual application, named *Visual MRI*, has been designed and developed, considering the main IV criteria and methodologies. Moreover, a novel unsupervised *cluster analysis* on $k$PS and $f$PV parameter spaces *and* on the tumor area topology (i.e., the *image* space) has been introduced, based on a non-parametric approach, named mean shift (MS) [21]; the leading idea is to create clusters composed by similar values of $k$PS and $f$PV, located in well defined areas in the MRI image space. The main underlying principle of MS is that the data space is regarded as an empirical probability density function to estimate. The MS procedure operates by shifting a fixed size estimation window, i.e. *the kernel*, from each data point towards a local mode, denoted, roughly speaking, as a high concentration of points. Points converging to the same mode are considered as belonging to the same region or cluster. Despite the quality of the obtained results shown in literature, it has to be pointed out that mean shift clustering relies on the tuning of several parameters, where a kernel is empirically specified. In general, the kernel is specified by the *shape* and the *bandwidth values* [21]: the former describes how strongly points are considered in the mode seeking procedure, while the latter defines the level of detail of the analysis. Large bandwidths lead to global but coarse separations, whereas small bandwidths better identify local modes, however risking over-partition.

In this paper, we introduce a robust automatic strategy that avoids any parameter setting, leading to a completely unsupervised segmentation procedure, named *MRI-mean shift* (MRI-MS). Furthermore, this permits *Visual MRI* to provide an effective and seamless integration among the visual interface and the clustering framework: in particular, a switch between the MRI image space and the parameter space is performed via *linked brushing* visualization methods. This makes easy understanding the nature of a cluster, observing its points in both the spaces. This investigation approach has been revealed to be particular useful for understanding the relationship between $k$PS and $f$PV parameters on some particular tumoral regions.

The rest of the paper is organized as follows. In Section 2 some basic concepts of IV are introduced, followed by discussions about the main IV approaches for MRI data and the main existing techniques for MRI data analysis. Section 3 gives details on the experimental data used in this work, highlighting also how $k$PS and $f$PV parameters are organized for the proposed application. The cluster analysis performed through *MRI-mean shift* is fully explained in Section 4. In Section 5 the methodological and design aspects of *Visual MRI* are described. Examples of real use of *Visual MRI* are reported in Section 6 and, finally, conclusions are drawn in Section 7.

## 2 Background and related work

In the following, we will briefly summarize the IV principles, the application of IV in medicine, and the state of the art of the MRI data analysis.

Graphical tools for visualizing data or knowledge are very useful for human perception [3]. In fact, by using *graphical aids*, people are able to overcome the natural challenges that are involved in the cognitive process [22]. In order to design and develop an effective IV framework, the *visualization process* needs to be carefully defined. It involves the stages from *raw data* transformation to visual and interactive *representation*. In particular, the visualization process is defined by *data transformation*, *visual mapping* and *view transformation*.

**Data transformation.** Raw data are transformed into data tables by carrying out some data processing techniques such as data set reduction, parameter computation, feature extraction, and so on. It is important to distinguish between *physical* and *non-physical* data. The first ones are spatially and temporally well defined. The latter ones are more general and need to be visualized through more complex representations.

**Visual mapping.** Transformed data need to be represented by effective visual structures. This phase is called *visual mapping*. Visual structures are characterized by the following components:

- **spatial substrate**: it defines how the space is organized into the visual representation. The space is described in terms of *axes* and their properties. Some elementary types of axes are: unstructured axis, nominal axis, ordinal axis and quantitative axis [3].
- **graphical objects or marks**: they are the basic components, such as points, lines, areas, volumes, of visual structures . Marks are characterized by *mark properties*, which influence the human perception. A typical exam-

ple of such properties are the so called *retina properties*: position, dimension, orientation, color, texture, and shape.

- **connection and enclosure**: they are visual components representing the relationship among the data appearing in the visual representation. They can evidence dynamic flows, tree or graph connections, logical sequences, and so on. A particular case of data relationship is given by the temporal connection.

An effective visual mapping consists of defining appropriate visual structures according to a specific application domain. In particular, data must be preserved and the visual representation must not lead to ambiguous interpretation.

**View transformations.** View transformations interactively modify and augment visual structures by establishing graphical parameters in order to improve the perception of the analyzed data. Some typical view transformations are:

- **location probes**: they allow the visualization of additional information by using some location in the visual structure. Typically, a *details on demand* approach is defined by displaying *pop-up windows* or *hierarchical menu*. An effective example of location probe is *linked brushing*, i.e., the cursor passing over one location creates visual effects to other markers [9]. In more details, a selection done in one view should be visible in another view, regardless the different dimensions that may be shown.
- **viewpoint controls**: they allow the change of the viewpoint, for magnifying visual structures and making details more visible. Commonly, affine transformations are introduced such as zooming, pan, and clipping the view-

point.

- **distortion**: it allows one to modify the physical properties of visual structures by creating focus-and-context views. Overview and details are combined into a single visual structure.

### *2.2 IV in medicine*

The main IV applications in medicine focus on effective data exploration [11], advanced rendering techniques [12], or immersive environments [13–15].

In [11], the authors propose an effective toolkit for the exploration of tomographic medical images on a computer screen by carefully designing three aspects: *control*, *navigation*, and *details in context*. *Control* provides the ability to interactively create user-defined image groups and to control group location, visibility, and display size. *Navigation* provides the capability of locating and relocating images. *Details-in-context* allows one to view one or more images up close while still viewing the remaining images.

In [12], a new medical volume rendering approach has been introduced for the clinical task of stenosis assessment. The authors have proposed to convey the uncertainty of the tissue classification in MR angiographies by animation methods. A probabilistic transfer function is defined which allows for direct user interaction with the classification. The rendering is animated by sampling the probability domain over time, which results in varying appearance for uncertain regions.

In [13, 14], Sorensen et al. have developed an interactive virtual reality visualization of cardiac magnetic resonance data allowing the surgeon and the

cardiologist to examine the heart in a 3D environment. The system is meant to give clinicians a better understanding of the patient's cardiac morphology, thus helping in the planning of cardiac interventions. In [15], the authors have proposed a method for fast and efficient analysis of dynamic MR image series of the female breast. A multidimensional real-time visualization system has been developed to display morphological and functional tissue information simultaneously by superimposing the computed functional tissue parameters on the anatomical information.

### *2.3 MRI data analysis*

As for DM techniques applied to MRI data, several work has been done, especially for MRI clustering, as in [16–18] to mention some proposals. Most proposed methods are based on the $K$-Means algorithm [7]. In [16], a quantitative comparison of MRI cluster analysis techniques has been performed and described. With respect to the proposed evaluation, results clearly shown that methods based on the neural gas algorithm [23] and on the $K$-Means one perform significantly better than all the other methods.

In [17, 18], variants of the $K$-Means have been introduced to the medical domain, based on the so called *fuzzy C-Means*(FCM) [23] technique. In particular, the FCM takes advantages from fuzzy logic algorithms to enhance clustering performances by allowing pixels to belong to multiple clusters with varying degrees of memberships. In [17], the clustering of MRI time series has been performed for the identification and separation of artifacts as well as for the quantification of expected novel information on brain activities. In [18] the authors focused on the methodological aspect of FCM by improving the

computation of the distance function which measures the similarity among voxels. The proposed approach has been tested for MRI-brain segmentation using both synthetic and real data.

However, as a matter of fact, $K$-Means (and in general, $K$-Means-like algorithms) is proven to be effective only in case of spherical Gaussian-shaped clusters; moreover, it requires that the number of clusters in the data must be specified a priori. While the $X$-Means approach solves the issue related to the specification of the number of clusters [24], the assumed shape of clusters still remains an open issue.

It is worth to note that in general all the methods presented above implicitly assume a given cluster geometry, which makes them unable to handle more complex or variable feature spaces. As a valid alternative, a clustering strategy which does not constrain the shape of clusters is built upon the mean shift (MS) paradigm [21]. This is an iterative technique which estimates the local modes of the multivariate distribution underlying the feature space, using a kernel function to locally analyze the data. The number of clusters is obtained automatically by finding the centers of the densest regions in the space, and the shape of clusters is obtained by calculating the basins of attraction of each mode.

In general, the kernel function is specified by the profile and the bandwidth values: the former describes how strongly the points are considered in the mode seeking procedure, and the latter defines the level of granularity of the analysis. Usually, the most used kernel shape is the Epanechnikov kernel [25], which ensures the finite convergency of the MS procedure. For what concerns the kernel width parameter, few strategies are present in literature that auto-

matically find an optimal width parameter. The most recent and used strategies are reported in [25], but the underlying hypothesis is that data are locally organized as multidimensional Gaussian distributions. Other techniques find optimal bandwidth values under the constraint that the input domain is one-dimensional, or composed by independent one-dimensional subdomains. As we will see in the following, this strategy can be *partially* applied to our problem.

More complex techniques have been proposed in [26–28] for DCE-MRI data analysis which are based on the *learning by example* paradigm [7, 23], that requires the user to specify manually the labels of a set of samples (i.e., the *training set*). In [26], an artificial neural network (ANN) architecture has been introduced for breast cancer analysis which combines unsupervised and supervised techniques for voxel-by-voxel classification of kinetic signals. In particular, *malignant*, *benign*, and *normal* voxels can be discriminated from a set of labeled examples without requiring the radiologists to define a mathematical model of the measured signals or of the underlying physiological process. In [27], the authors have focused on the same medical problem and proposed an evaluation of radiological features for tumors classification by exploiting several machine learning methods. In particular, they exhaustively evaluated both morphological and kinetic attributes of DCE-MRI signals. In [28], the authors have proposed to project the multidimensional DCE-MRI signal space of breast cancer data into a subspace of lower dimension, in order to obtain a more compact representation of the source data. The visualization of such data projection allows the users to improve the visual data exploration with regard to the differentiations between benign and malignant lesions.

## 3 Structuring the DCE-MRI data set for IV and DM

Aim of considered DCE-MRI experiments is to determine in a non-invasive fashion the *fractional plasma volume* ($f$PV) of tumor tissue and the *endothelial permeability* ($k$PS) of tumor vasculature, which are accepted surrogate markers of angiogenesis.

HT-29 human colon carcinoma fragments were implanted subcutaneously in the flank of 10 nude mice weighing approximately 25 g. Animals were inserted in the study when the tumors reached a weight of approximately 500 mg as estimated by calliper measurements of tumor diameters [20].

DCE-MRI experiments were performed by acquiring a series of MR images before and at different time points after the injection of the contrast agent, Gd-DTPA-albumin [29]. A total of 24 images were acquired (covering a time interval of 53 min). The contrast agent was administered in bolus during the time interval between the first and the second image. The plasma kinetic of Gd-DTPA-albumin was determined ex vivo by measuring longitudinal relaxation time values of blood samples withdrawn from normal mice at different time point after contrast agent administration.

The dynamic evolution of the signal intensity in MR images is analyzed using a two compartments tissue model [30], in which the contrast agent can freely diffuse between plasma and interstitial space. $k$PS and $f$PV values are obtained pixel by pixel by fitting the theoretical expression to experimental data [20]. In this work experiments were performed in order to assess the antiangiogenic effect of a specific drug. Data analysis was adapted from [30] for the special case of a macromolecular contrast agent [20].

Four spatial substrates have been defined: the physical space, the $k$PS space, the $f$PV space, and the parameter space.

- **physical space**: the physical space is a volumetric space. As usual for MRI data sets, data are visualized through a 2D image (the MRI image) that is obtained by selecting a slice of the whole volume. Each pixel of the image represents the intensity of the MRI signal.
- **$k$PS and $f$PV space**: the considered parameters $k$PS and $f$PV, previously described, are derived from MRI slices applying the pharmacokinetics model introduced in [19]. For each pixel of a selected MRI image there is a value for $k$PS and $f$PV, respectively. Therefore, two parameter maps are derived, representing the $k$PS and $f$PV spaces, respectively.
- **parameter space**: in order to obtain a unified representation of the $k$PS and $f$PV maps, a further space is defined. Two quantitative axes have been introduced ($k$PS for horizontal and $f$PV for vertical axis). Then, the physical image has been scanned and for each pixel $x_i$ the two values $kPS_i$ and $fPV_i$ are observed. Thus, after the projection of all the 2D points $p_i(kPS_i,fPV_i)$ the *parameter* space is obtained.

*Cluster analysis*, as it will be detailed in the next section, is performed on a *joint* domain, which is composed by the physical space and the parameter space: afterwards, a suitable visualization of clustering results is provided in all the considered spaces, to allow the physician to relate a given cluster to its anatomical location, and viceversa.

Figure 1 shows the designed interaction among the involved spatial substrates. From the selected region on the physical space, both the $k$PS and $f$PV maps are computed (see interactions $A.1$ and $A.2$ in Figure 1). Therefore, the pa-

rameter space is composed (see interactions $B.1$ and $B.2$ in Figure 1) and clusters are detected. Finally, the identified clusters are re-projected to the physical space (see interaction $C$ in Figure 1).

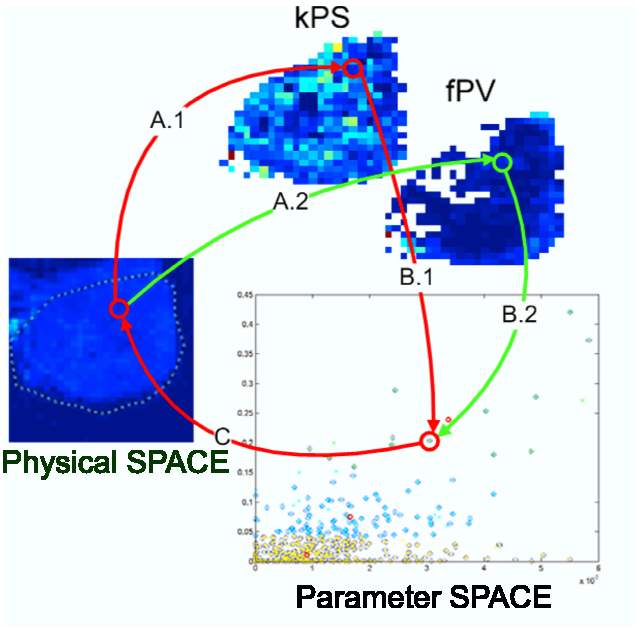


Fig. 1. Spatial substrates and their interactions: a given pixel and its corresponding representation in the different spaces is depicted together with the suitable interaction.

## 4 Cluster Analysis

In this section we will introduce an overview of the MS algorithm. Theoretical aspects will be described by focusing on the current approaches for the automatic free-parameter estimation. Indeed, the proposed version of the MS clustering will be introduced by highlighting the strategy for the automatic bandwidth selection on each available subspace.

*4.1 Overview of the mean shift algorithm*

The MS procedure is a dated, recently re-discovered, non-parametric density estimation technique [21, 31]. The theoretical framework of the MS arises from the Parzen Windows technique, that, in particular hypotheses of regularity of the input space (such as independency among dimensions [21]), estimates the density at point $\mathbf{x}$ as:

$$\hat{f}_{h,k}(\mathbf{x}) = \frac{c_{k,d}}{nh^d} \sum_{i=1}^{n} k\left(\left\|\frac{\mathbf{x}-\mathbf{x}_i}{h}\right\|^2\right) \tag{1}$$

where $d$ indicates the dimensionality of the data processed, $n$ is the number of points available, and $k(\cdot)$ is the kernel profile, that models how strongly the points are taken into account for the estimation, in dependence with their distance to $\mathbf{x}$, influenced by the $h$ term. Finally, $c_{k,d}$ is a normalizing constant, depending on the dimensionality of the data and on the kernel profile.

MS extends this "static" expression, differentiating (1) and obtaining the gradient of the density, which is:

$$\nabla \hat{f}_{h,k}(\mathbf{x}) = \frac{2c_{k,d}}{nh^d}\left[\sum_{i=1}^{n} g\left(\left\|\frac{\mathbf{x}_i-\mathbf{x}}{h}\right\|^2\right)\right]\left[\frac{\sum_{i=1}^{n}\mathbf{x}_i g\left(\left\|\frac{\mathbf{x}_i-\mathbf{x}}{h}\right\|^2\right)}{\sum_{i=1}^{n} g\left(\left\|\frac{\mathbf{x}_i-\mathbf{x}}{h}\right\|^2\right)} - \mathbf{x}\right] \tag{2}$$

where $g(x) = -\frac{\partial k(x)}{\partial x}$. In the above equation, the first term in square brackets is *proportional* to the normalized density gradient, and the second term is the MS-*vector* $M_v(\mathbf{x})$, that is guaranteed to point towards the direction of maximum increase in the density [21].

Therefore, starting from a point $\mathbf{x}^{(j)}$ in the feature space at the iteration $j$, the iteration

$$\mathbf{x}^{(j+1)} = M_v(\mathbf{x}^{(j)}) + \mathbf{x}^{(j)} \tag{3}$$

defines a path leading to a stationary point $\mathbf{y}$ of estimated density. The modes of the density are such stationary points. This MS procedure is guaranteed to converge in a finite number of iterations [21].

In the MS-based clustering, hereinafter simply MS clustering, the first step is made by applying the MS procedure to all the points $\{\mathbf{x}_i\}$, producing the convergency points $\{\mathbf{y}_i\}$. A consistent number of close convergency locations, $\{\mathbf{y}_i\}_l$, indicates a mode $\mu_l$. The clustering operation consists in marking the corresponding points $\{\mathbf{x}_i\}_l$ that produces the set $\{\mathbf{y}_i\}_l$ with the label $l$. This happens for all the convergency location $l = 1, 2, \ldots, L$.

In this clustering framework, the only interventions required by the user involve the choice of the kernel profile $k(\cdot)$ and the choice of the bandwidth value $h$. For what concerns the profile of the kernel, the choices most adopted are the Gaussian profile and the Epanechnikov profile [21]; this last one has the desirable property that ensures the MS procedure is convergent in a finite number of steps. In order to produce a robust application, we chose thus the Epanechnikov profile, or Epanechnikov kernel, described by the following function:

$$k(x) = \begin{cases} 1 - x & \text{if } 0 \leq x \leq 1 \\ \\ 0 & \text{otherwise} \end{cases} \tag{4}$$

that, if differentiated, leads to the uniform kernel $g(\cdot)$, i.e. a $d$-dimensional unit sphere.

The kernel bandwidth parameter regulates the level of detail with which the data space is analyzed; a large bandwidth means general analysis (few convergency locations), while a small bandwidth leads to a finer analysis (many

convergency locations). As we will see in the following, setting the kernel bandwidth value could require a strong effort by the user: therefore, strategies to automatically determine the kernel bandwidth have been recently studied [25, 32].

A crucial problem of all the strategies that find a global bandwidth value is that, when the local characteristics of the feature space differ significantly across data, it is difficult and unnatural to find a unique optimal global bandwidth value. Therefore, the MS clustering framework has been adapted in the so called "variable mean shift", or "sample point mean shift estimator", in which the kernel bandwidth varies, depending on the considered point. Briefly speaking, the MS vector becomes

$$M_v(\mathbf{x}) = \frac{\sum_{i=1}^{n} \frac{\mathbf{x}_i}{h_i^{d+2}} g\left(\left\|\frac{\mathbf{x}_i - \mathbf{x}}{h_i}\right\|^2\right)}{\sum_{i=1}^{n} \frac{1}{h_i^{d+2}} g\left(\left\|\frac{\mathbf{x}_i - \mathbf{x}}{h_i}\right\|^2\right)} - \mathbf{x} \tag{5}$$

where $h_i = h(\mathbf{x}_i)$ denotes the width of the bandwidth at point $\mathbf{x}_i$.

Roughly speaking, there are two main approaches addressing the adaptive bandwidth selection: (i) the *non-parametric* MS [32], and (ii) the *Gaussian* MS bandwidth estimators [25]. The first one [32] is based on the minimization of the mean integrated squared error (MISE) by inserting a plug-in rule into the MS clustering strategy [33]. In general, plug-in rules consist in "plugging in" bandwidth estimates which minimize different kind of estimation errors evaluated on the *entire* pool of data [34]. Here, the plug-in rule gives an initial optimal *global* fixed bandwidth value, which is locally modified by the MS strategy. Although this approach works well for one dimensional data spaces, it becomes really hard to manage in the case of multidimensional data spaces.

The *Gaussian* MS bandwidth estimator [25] is build upon the assumption that data to analyze are locally Gaussian. The estimator fits sequentially at each sample point a set of Gaussian kernels with increasing bandwidth, looking for the bandwidth for which the intensity of the MS vector is maximized. This approach is suitable for higher dimensional spaces, but it is not feasible when the Gaussian hypothesis on data distributions is not verified.

### *4.2 The proposed method:* MRI-Mean Shift

In this paper, we consider each point $\mathbf{x}_i$ of the source data as a 4D entity, living in a *joint domain*. Specifically, $\mathbf{x}_i = [\mathbf{x}_{i,s}, \mathbf{x}_{i,k\mathrm{PS}}, \mathbf{x}_{i,f\mathrm{PV}}]$, where $\mathbf{x}_{i,s}$ identifies the 2D pixel coordinates of a point of the MRI image (the physical space or subdomain), $\mathbf{x}_{i,k\mathrm{PS}}$ identifies the $k$PS subdomain, and $\mathbf{x}_{i,f\mathrm{PV}}$ addresses the $f$PV subdomain.

In order to perform clustering in the joint space, a multivariate *product* kernel profile is used [21], that is:

$$\tilde{k}_{h_s,h_{k\mathrm{PS}},h_{f\mathrm{PV}}}(\mathbf{x_i}) = \prod_{u\in\{s,k\mathrm{PS},f\mathrm{PV}\}} k\left(\left\|\frac{\mathbf{x}_{i,u}}{h_{i,u}}\right\|^2\right) \tag{6}$$

where $h_{is}, h_{ik\mathrm{PS}}, h_{if\mathrm{PV}}$ are the kernel bandwidths for each subdomain applied to the Epanechnikov kernel, whose value varies depending on the location of point $\mathbf{x}_i$.

The use of the product kernel enforces to search for dense zone in the joint space, adopting a particular level of detail for the analysis (i.e. a particular

kernel bandwidth) for each subdomain and for each point location. A location in which data are organized in several small compact groups should have a small bandwidth, in order to highlight all the small details. A location in which there is a single or few bigger modes should have a large bandwidth, in order to capture in a better way big shapes. Choosing the right kernel bandwidth for each location and for each subdomain turns out to be a time consuming try-and-test procedure, that behaves badly in a serial work session.

Aiming at creating an effective and efficient MRI analysis tool for physicians, we decided to automatize the task of the bandwidth selection [1] . Therefore, we select for each subdomain the more appropriate bandwidth selection method.

### *4.2.1 Estimating the $h_{i,kPS}$ and $h_{i,fPV}$ bandwidth parameters*

To estimate the $h_{i,k\mathrm{PS}}$ and $h_{i,f\mathrm{PV}}$ bandwidth parameters, we need to select the most suitable method among those described above. In Figure 2 a) and b) typical examples of MRI values of $k$PS and $f$PV subdomains are visualized as histograms. In general, data exhibit an irregular structure (consider, for example, the first mode on the left of Figure 2 a), and the smaller peaks on the right). Thus, since these distributions are clearly non-Gaussian, the *Gaussian* MS bandwidth estimator [25] should not be applied. Moreover, we consider the fact that, since the two parameters (i.e., $k$PS and $f$PV) refer to independent physical phenomena, the respective bandwidth estimations can be carried out by two independent mono-dimensional processes. For this reason, we employ in these two subdomains the non parametric MS bandwidth estimation as

[1] anyway, in *Visual MRI* we included also the option of manually setting bandwidth parameters.

described in [32], obtaining for each sample $i$ the values $h^{\text{BEST}}_{i,k\text{PS}}$, $h^{\text{BEST}}_{i,f\text{PV}}$

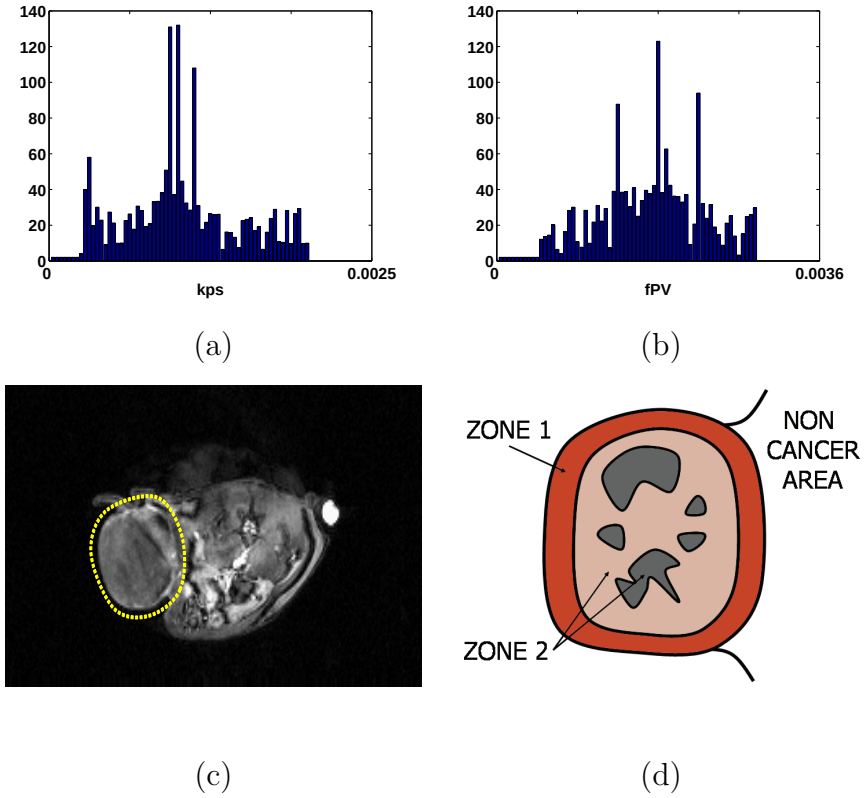


Fig. 2. MRI subdomains: histogram representations of the (a) $k$PS and (b) $f$PV subdomains; in c), the physical subdomain is represented, where the cancer area is highlighted by the dotted line; in (d) the typical expected partition of the cancer area is shown.

### *4.2.2 Estimating the $h_{i,s}$ bandwidth parameter*

To estimate the bandwidth $h_{i,s}$, we need to analyze the shape of the expected clusters into the spatial subspace. Figure 2 c) depicts the physical space, i.e. the MRI image; on the bottom-left the tumoral area is highlighted by the dotted line. In general, independently from the kind and from the shape of the tumoral area, the zones expected by the physicians to form separate clusters are mainly two (Figure 2 d)): the first one is the border area (ZONE 1),

i.e., a stripe-shaped area, highly vascularized, connected to non-cancer zones. This is supposed to be the zone playing the most active role in the development of the tumor, and its exact discovery results crucial for a well-located antiangiogenic treatment. The second one (ZONE 2) is the internal part of the tumor, usually formed by isolated sub-clusters of necrotic matter merged in a weakly vascularized substrate. These two 2D areas are highly irregular and the hypothesis of local Gaussian shape of data does not hold, thus making unsuited any automatic bandwidth value selection strategy based on Gaussian hypothesis [25]. Moreover, also the non parametric MS bandwidth method is not applicable since the $\mathbf{x}_{i,s}$ sub-domain lies on a domain higher than 1, with non-independent components.

Supposing we are given the optimal bandwidth values $h^{\mathrm{BEST}}_{i,k\mathrm{PS}}$, $h^{\mathrm{BEST}}_{i,f\mathrm{PV}}$ by the procedure previously explained, we propose here a new task-oriented bandwidth selection technique for the physical subspace $\mathbf{x}_{i,s}$, that exploits decomposition stability criteria. A *stable* segmentation or partition is a segmentation maintaining the same number of clusters while varying the free parameters involved (in this case the bandwidth values) [31]. The technique is composed by three steps.

(1) *Standardization*: we rearrange the physical sub-domain as a hypercube, where the length of the side is fixed at the value $R_s$, indicating the largest dimension of that subspace.
(2) *Evaluation of bandwidth candidates*: as candidate bandwidth values $h_s^{(v)}$, we set $N_{\max}$ values, ranging uniformly from $h_s^{(1)} = R_s/N_{\max}$ to $h_s^{(N_{\max})} = R_s/2$.

With these values, we perform the Mean Shift clustering with the prod-

uct kernel of Eq. (6) with bandwidth values $h_{i,k\mathrm{PS}}^{\mathrm{BEST}}$, $h_{i,f\mathrm{PV}}^{\mathrm{BEST}}$,$h_{i,s}^{(v)}$, where $\forall i$, $h_{i,s}^{(v)} = h_s^{(v)}$, (in the following, we will use thus $h_s^{(v)}$ for clarity).

(3) *Best bandwidth choice*: After these trials, we choose as best bandwidth value for the spatial subdomain $h_s^{BEST}$, where $BEST = \lceil (v_{\max} - v_{\min})/2 \rceil$ indicates the bandwidth value in the center of the largest range of bandwidth values $[h_s^{(v_{\min})}, h_s^{(v_{\max})}]$ over which the Mean Shift clustering gives the same number of clusters for the given data (i.e., a plateau, as depicted in Figure 3).

This method identifies thus the most stable global bandwidth, in the intuitive sense claimed by [31].

The partition obtained with the set of bandwidths $h_{i,k\mathrm{PS}}^{\mathrm{BEST}}$, $h_{i,f\mathrm{PV}}^{\mathrm{BEST}}$, $h_{i,s}^{\mathrm{BEST}}$ is the final result of our clustering technique.

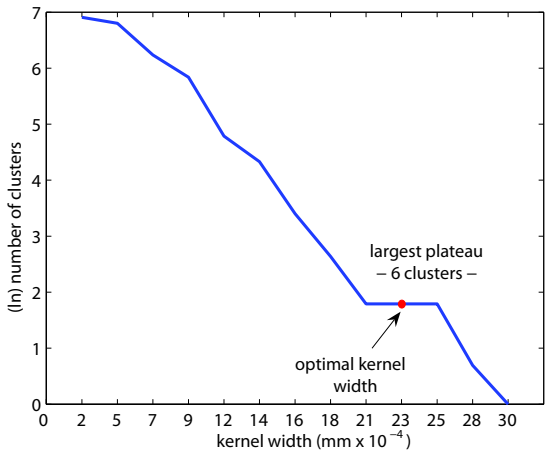


Fig. 3. Best bandwidth choice: in the scheme are reported the number of clusters (shown here under natural-logarithmic scale for a better understanding) resulting by the application of the mean shift clustering using different spatial kernel bandwidths. The largest plateau is clearly visible: in the middle of it the best kernel bandwidth is selected, that gives rise to $e^{1.7918} = 6$ clusters.

In order to evaluate the performances of our clustering technique, we performed a set of tests (10 subjects with 24 clusters each), where:

(1) we applied the MRI-MS without considering the physical space: the resulting segmentations are clearly oversegmented (an example is shown in Figure 4 (a)). This is due to the fact that the modelling of the physical space induces a constraint on the compactness of the clusters produced;

(2) we applied the MRI-MS adopting the parametric gaussian bandwidth selection proposed in [25], which implies the underlying presence of gaussian-shaped clusters: also in this case the results are oversegmented, organized as small gaussian clusters (as depicted in Figure 4 (b)).

(3) We applied our technique, whose result (the same of Figure 13) is shown in Figure 4 (c).

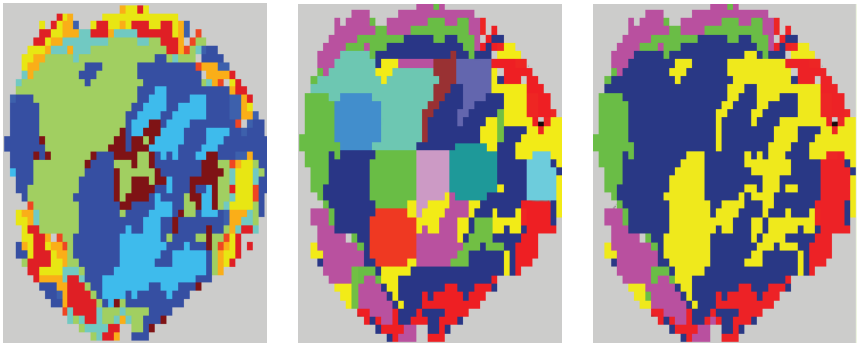

(a) (b) (c)

Fig. 4. Compared results: (a) MS clustering without the physical space (b), cluster with a parametric gaussian bandwidth for the spatial domain (c) clustering by the proposed technique

Our technique produces best results, in the sense that a clear correspondence is present between the obtained clusters and the expected physiological organization of the tumor.

## 5 The visual interface

The visual interface of *Visual MRI* has been designed according to IV principles. Figure 5 shows a screenshot of the main window. The MRI image (i.e., the selected slice of the volumetric space) is displayed in the central part of the window (area 1 in Figure 5). The general (textual) information related to the experiment is shown in the upper left side (area 2).

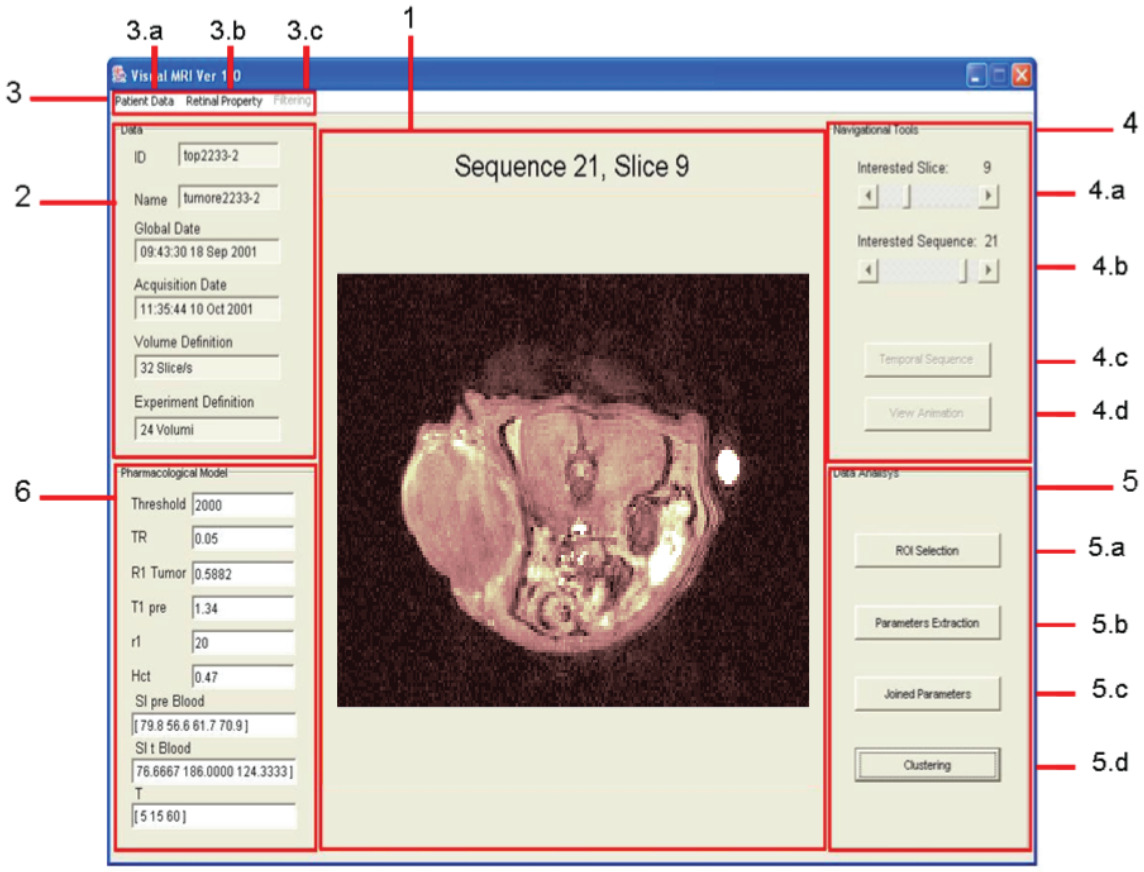


Fig. 5. Main interface of *Visual MRI*: the main areas of the interface are enumerated.

Then, available options are:

- **slice selection and animation**. Each slice (2D) of the MRI physical volume (3D) can be visualized by tuning a slide bar for the volume (area 4.a)

and a slide bar for the time (area 4.b). Moreover, the whole sequence of a single acquisition can be also displayed as a movie (area 4.c). Furthermore, the diffusion of the contrast agent can be monitored by selecting a slice and visualizing its variation along the time (area 4.d).

- **modification of retinal properties**. It is possible to modify either a single color or a predetermined color map. Furthermore, the shape of marks can be customized. All the retina properties modifications can be obtained by the main menu (area 3.b).
- **noise removal**. Classical noise filters can be applied to the acquired MRI signal, such as gaussian and median filters. This option can be carried out on both each 1D signal along the time space and each 2D image slice (area 3.c).
- **region of interest (ROI) selection and zooming**. The user may select manually a region of interest (area 5.a). By combining this option with zooming, an exhaustive analysis of some details of the image is allowed.
- **parameter map extraction**. The $k$PS and $f$PV parameter maps can be extracted by clicking a suitable button (area 5.b). Then, a further button allows the switching among the two images. Some constants of the pharmacokinetics model can be manually tuned (area 6).
- **parameter space projection and clustering**. By selecting the button in the area 5.c, the parameter space can be displayed. Furthermore, as described in Section 4, clusters are automatically detected (area 5.d). After the clustering step, the user can switch between the physical and the parameter space. A sort of *bidirectional* linked brushing has been proposed. Indeed, by selecting a region into the physical space, the parameter distribution on the parameter space is highlighted (*straight* linked brushing). On the other hand, by selecting a cluster in the parameter space, the corre-

sponding regions on the physical space appear (*reverse* linked brushing). The bidirectional linked brushing can be applied also in a local way: selecting a point in a particular space, it is possible to visualize it in all the other spaces, highlighting its coordinates and the associated value in that space (the MRI intensity in the physical space, the $f$PV and $k$PS values in the respective spaces and the cluster label in the parameter space).

## 6 *Visual MRI* at work

In this section some selected examples of the use of *Visual MRI* are reported from the set of experimental data described in Section 3. After data acquisition, raw data are available and data preprocessing is carried out by applying noise removal operators.

Furthermore, through volumetric browsing, details on demand, and coloring techniques, a preliminary analysis of data is given. Figure 6 shows three pictures of an MRI slice after data selection. The leftmost image is in black and white, while the other ones are obtained by changing the color setting.

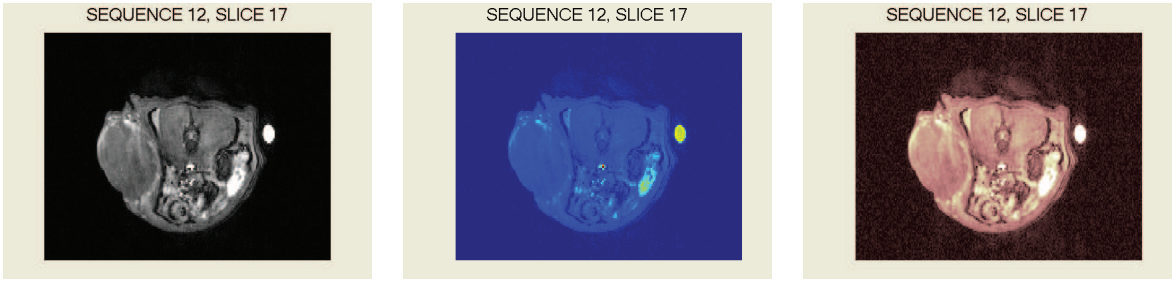


Fig. 6. A slice of MRI data set. The leftmost image is in black and white, while the other ones are obtained by changing the color setting.

In order to analyze the parameter values on the tumor, a region of interest

needs to be selected. The tumoral area is manually selected by using the ROI operator (the location of the tumoral area is a priori known). Figure 7 shows the ROI selection process. Then, the pharmacokinetics model is applied and the parameter maps are extracted (with respect to the selected area). Figure 8 shows the two parameter maps.

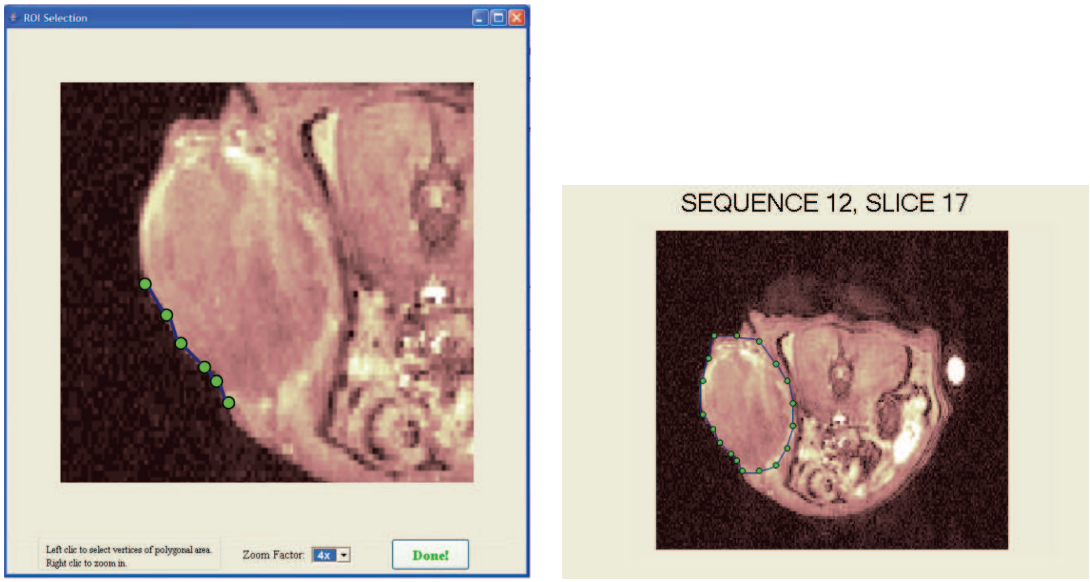


Fig. 7. An example of ROI selection by using the zooming operator (left) and the selected region (right).

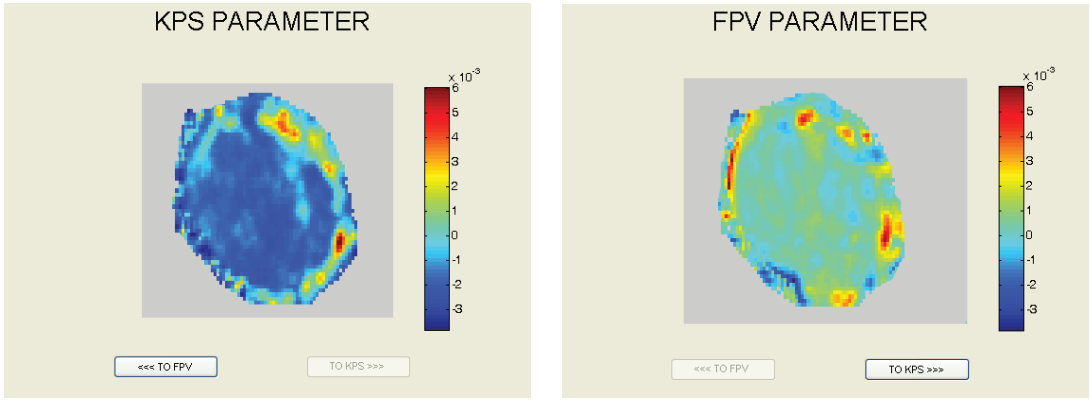


Fig. 8. $k$PS(left) and $f$PV(right) maps.

The next step is the core of our framework: the selected region is mapped into the *parameter* space and the more significative clusters are collected by carrying out the MRI Mean Shift cluster detector operator. Figure 9 shows

the parameter space before and after the cluster detection, respectively. This phase realizes a *straight* linked brushing (from physical space to parameter space).

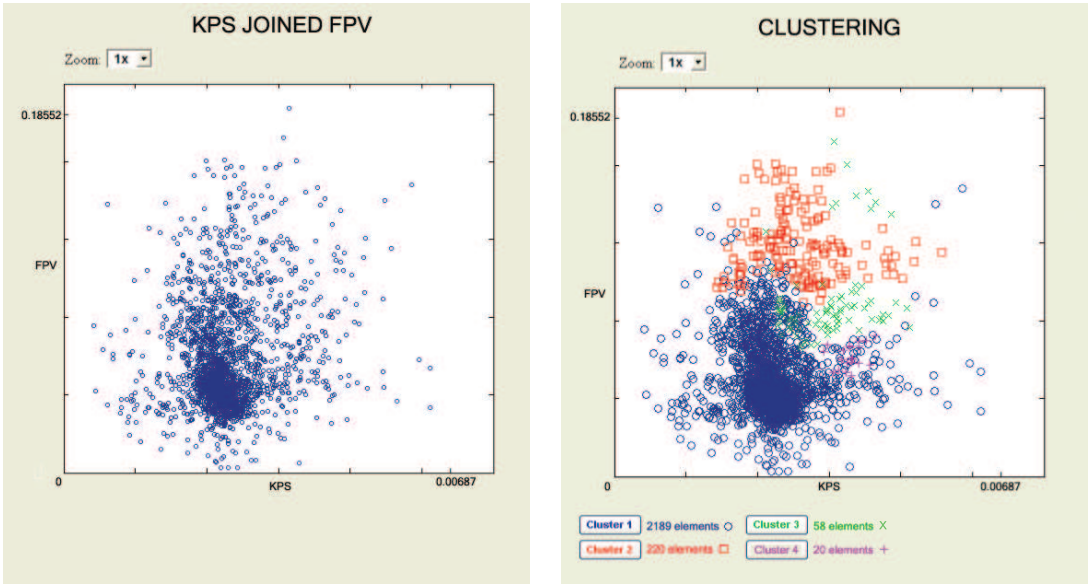


Fig. 9. Parameter space before and after cluster detection.

Therefore, selected clusters are re-projected into the physical space, evidencing some slice regions of the cancer area. This phase realizes a *reverse* linked brushing (from parameters space to physical space). Figure 10 highlights the tumoral regions inferred by the proposed approach.

In all the performed experiments, cluster analysis via MRI Mean Shift provided an effective subdivision of the tumor tissue in different clusters. In particular, the biggest cluster covers the whole interior of the tumor which is characterized by low values of $f$PV and $k$PS. The other clusters contain in general a limited number of pixels with highest values of $f$PV. These results are relevant from the medical point of view since regions detected by reverse linked brushing correspond to typical subdivision of the tumoral area expected by the medical scientists. In fact, as already described in Section 4.2.2, these tumors

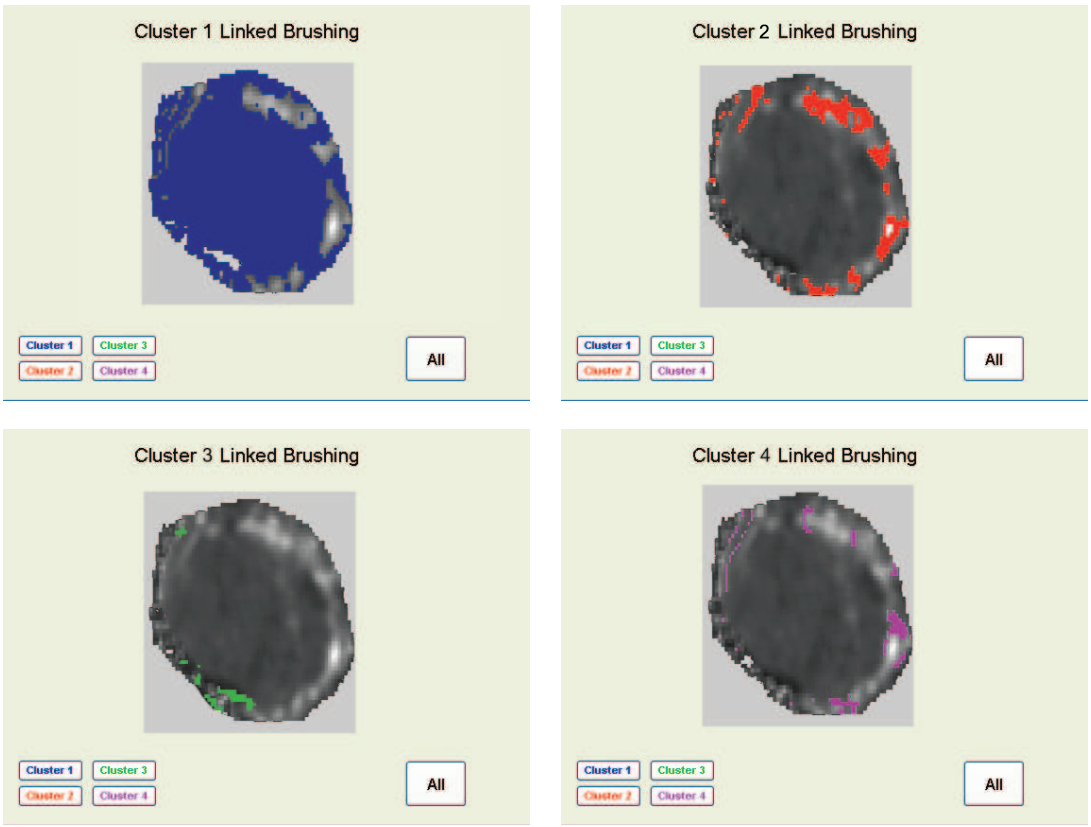


Fig. 10. Tumoral regions inferred by the proposed approach.

are characterized by an external well-vascularized rim, composed by a viable tumor tissue, and by an internal, scarcely vascularized necrotic area [20].

*Visual MRI* has been tested on several subjects by observing the same aspect of the cluster distribution on the tumoral region (Figures 11-14 show the use of *Visual MRI* on further three subjects, on different slices).

*Visual MRI* has been developed in Java 1.4 for Window XP. The analysis of a single slice requires from 1 to 5 minutes, while the study of an entire subject takes around 20 minutes.

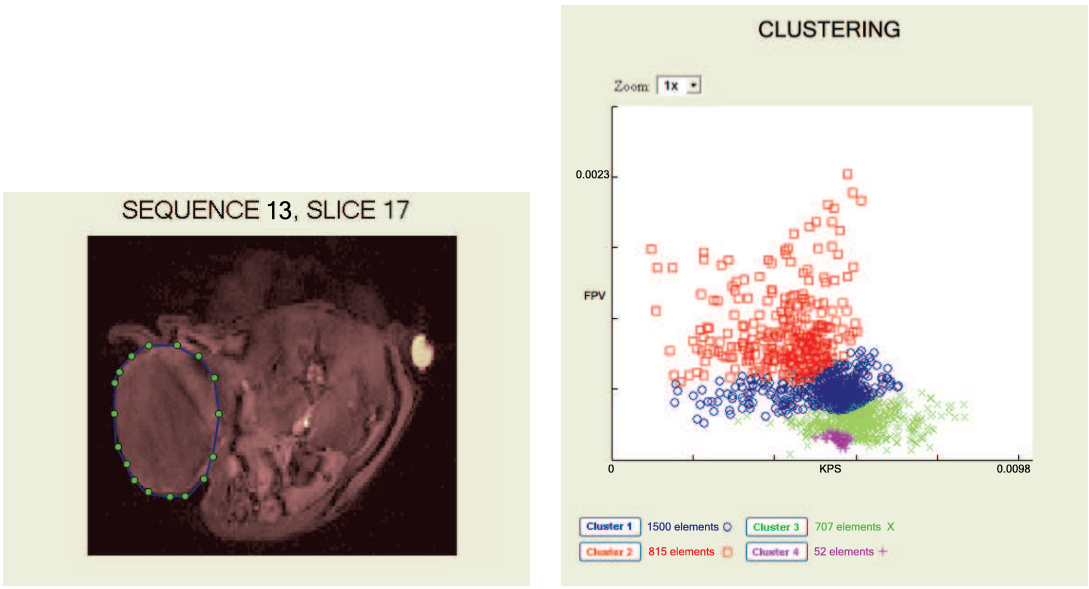


(a) (b)

Fig. 11. Example 2: MRI selected region (a), parameter space after clustering (b)

**Medical Relevance and Validation**

*Visual MRI* has proven to be useful for medical scientists to improve the analysis of DCE-MRI data sets. By this software system, the influence of $k$PS and $f$PV parameters for the characterization of tumoral regions has been verified, allowing physicians to validate the hypothesis about possible relationships between tumor angiogenesis and tumor microvessels.

In order to certify the meaning of the obtained clusters, an histological exam has been performed by physicians. In particular, 8 slices for 3 subjects analyzed and segmented by our method have been physically recovered, by killing the test animals. Successively, portions of tissues (randomly chosen) corresponding to the clusters identified by our algorithm have been visually analyzed by experts who confirmed the correctness of the obtained subdivisions (an example is shown in Figure 15).

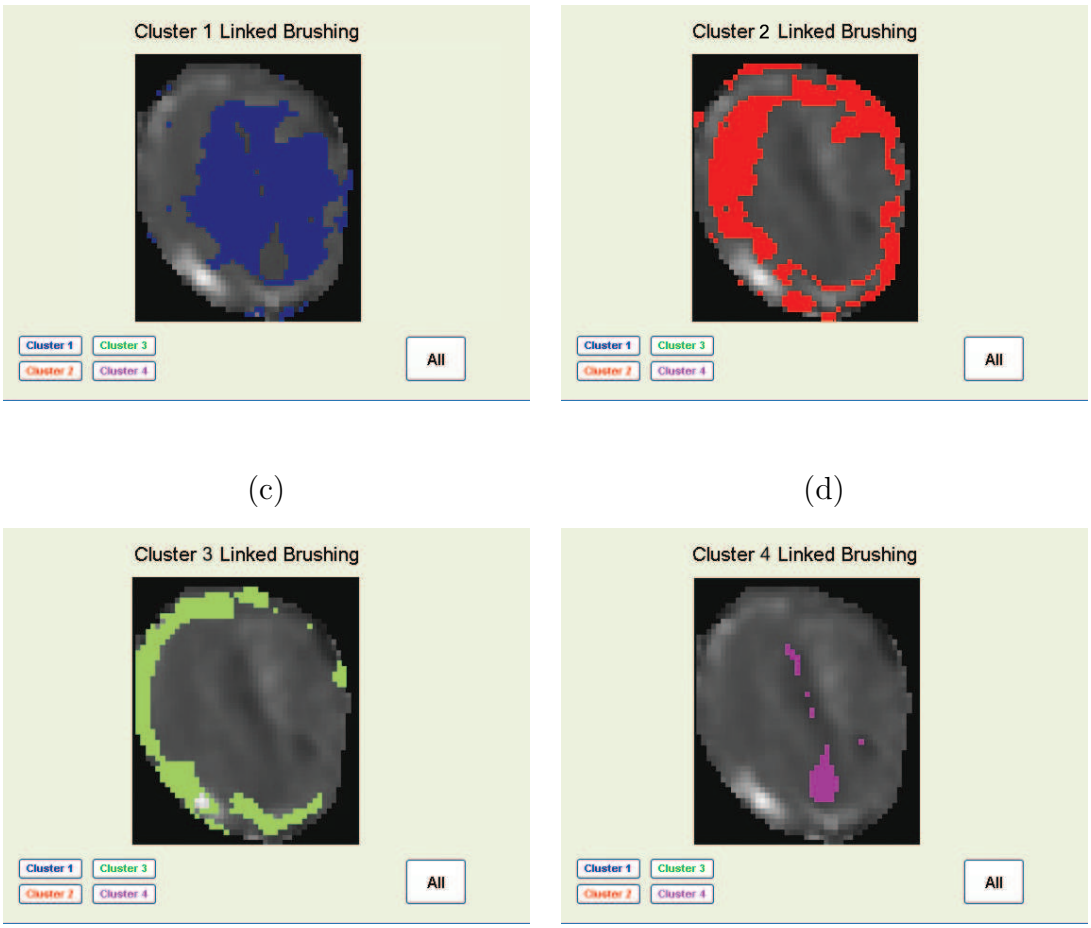


(c) (d)

(e) (f)

Fig. 12. Example 2: the four extracted clusters (c, d, e, f).

Once the proposed application has been validated on this subset of available samples, *Visual MRI* has been used as a tool for the verification of the vascular properties of the analyzed tumors without necessarily applying histological analysis on samples (which turns out to be highly sophisticated and time consuming).

Finally, although a systematic evaluation of usability of *Visual MRI* is difficult, due to the restricted number of expert scientists working on this kind of experimental issues in a single research unit, we involved the medical researchers in a detailed evaluation of Visual MRI, through some exhaustive

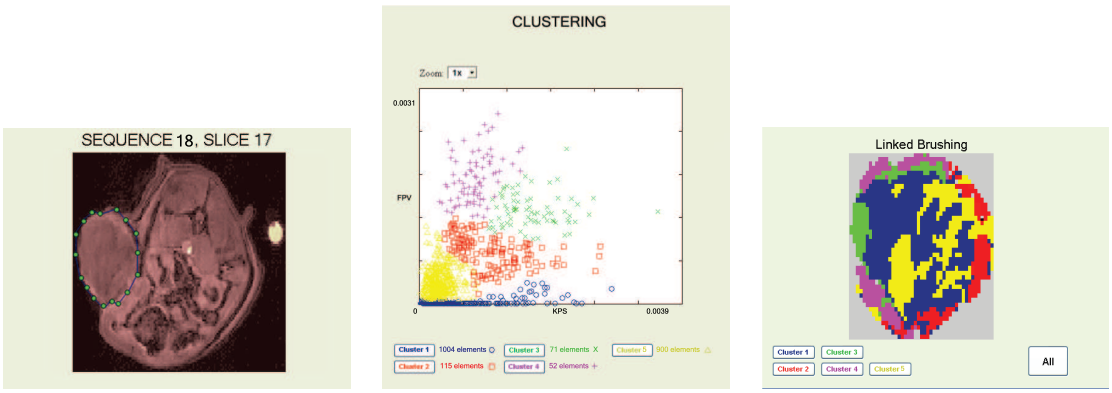


(a) (b) (c)

Fig. 13. Example 3: MRI selected region with the overall slice (a), parameter space after clustering (b) and the resulting segmentation (c).

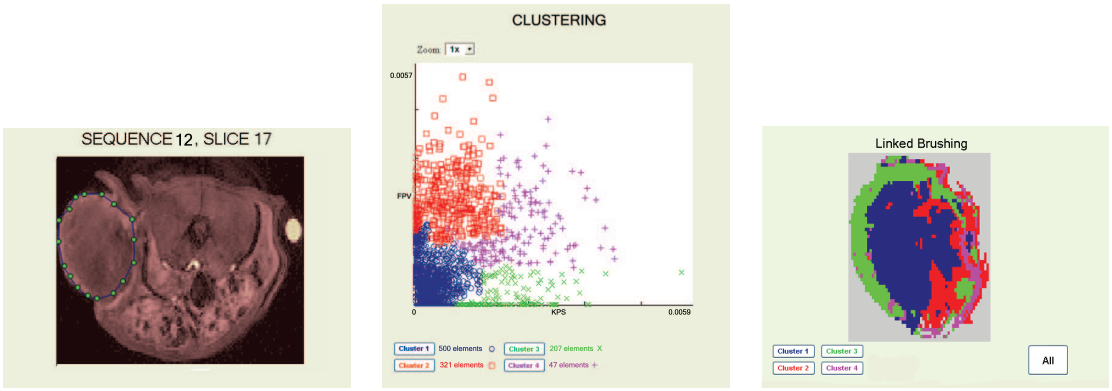


(a) (b) (c)

Fig. 14. Example 4: MRI selected region with the overall slice (a), parameter space after clustering (b) and the resulting segmentation (c).

work sessions and extended meetings and interviews. The three involved medical researchers have declared their comfortableness in using *Visual MRI* for both the graphical design and the intuitiveness of the interaction paradigms.

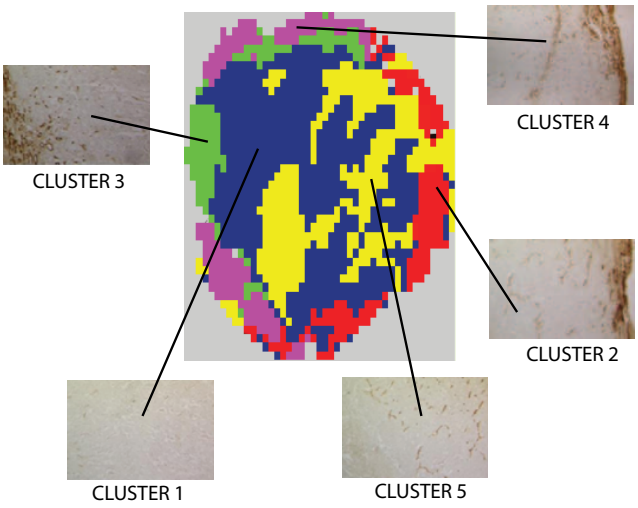


Fig. 15. Histological counterproof: the slice from which we obtained the shown segmentation (the same presented in Figure 13), has been surgically extracted by the test animal, and portion of tissue have been analyzed. Above, some portions of the tissue are visualized: as expected, cluster 1 and cluster 5 represent internal necrotic area, while the other clusters model highly vascularized zones.

## 7 Conclusions

In this paper a new software tool for DCE-MRI data analysis, *Visual MRI*, is proposed, aiming at improving the support of medical scientists in the context of research on cancer therapies: results show its effectiveness for the comprehension of dependencies between the analyzed parameters and the known tumoral regions. By *Visual MRI* we promote an effective merging of Information Visualization techniques and a novel Data Mining algorithm. In particular, (i) we embed in the application a linked brushing technique, which establishes a bidirectional connection among different visual representations of DCE-MRI data sets; (ii) we detail a novel data mining technique, by defining the MRI-MS algorithm for cluster analysis. This method introduces the *mean-shift* paradigm on MRI data by exploiting a new approach for the automatic bandwidth

selection.

*Visual MRI* has been successfully validated by the medical researchers since the extracted clusters correspond to expected tumoral subdivisions. Therefore, medical researchers use *Visual MRI* for the verification of connections between tumor microvessels and tumoral angiogenesis whose local treatments could lead to an easily endurable and more effective cancer therapy.

## References


[1] M. C. Ferreira de Oliveira and H. Levkowitz. From visual data exploration to visual data mining: a survey. *IEEE Transactions on Visualization and Computer Graphics*, 9(3):207–216, 2003.

[2] R. Spence. *Information Visualization*. ACM Press/Addison-Wesley, New York, USA, 2001.

[3] S. K. Card, J. D. Mackinglay, and B. Shneiderman. *Readings in Information Visualization - Using Vision to Think*. Morgan Kaufmann, San Francisco, USA, 1999.

[4] E. R. Tufte. *Envisioning Information*. Graphics Press, Cheshire, USA, 1990.

[5] M. R. Stytz, G. Frieder, and O. Frieder. Three-Dimensional Medical Imaging: Algorithms and Computer Systems. *ACM Computing Survey*, 23(4):421–499, 1991.

[6] L. Chittaro. Information visualization and its application to medicine. *Arificial Intelligence in Medicine*, 22(2):81–88, 2001.

[7] J. Han and M. Kamber. *Data Mining: Concepts and Techniques*. Morgan Kaufmann, San Francisco, USA, 2001.

[8] N. Lavrac. Selected techniques for data mining in medicine. *Artificial Intelligence in Medicine*, 16(1):3–23, 1999.

[9] D. A. Keim. Information visualization and visual data mining. *IEEE Transactions on Visualization and Computer Graphics*, 7(1):100–107, 2002.

[10] L. Chittaro, C. Combi, and G. Trapasso. Clinical data mining: a visual approach and its application to hemodialysis. *Journal of Visual Languages and Computing*, 14(6):591–620, 2003.

[11] J. E. Van der Heyden, K. M. Inkpen, M. S. Atkins, M. Sheelagh, and T. Carpendale. Exploring presentation methods for tomographic medical image viewing. *Artificial Intelligence in Medicine*, 22(2):89–109, 2001.

[12] C. Lundstrom, P. Ljung, A. Persson, and A. Ynnerman. Uncertainty visualization in medical volume rendering using probabilistic animation. *IEEE Transactions on Visualization and Computer Graphics*, 13(6):1648–1645, 2007.

[13] T. S. Sorensen, S. V. Therkildsen, P. Makowski, J. L. Knudsen, and E. M. Pedersen. A new virtual reality approach for planning of cardiac interventions. *Artificial Intelligence in Medicine*, 22(3):193–214, 2001.

[14] T. S. Sorensen, E. M. Pedersen, O. K. Hansen, and K. Sorensen. Visualization of morphological details in congenitally malformed hearts: Virtual, three-dimensional reconstruction from magnetic resonance imaging. *Cardiology in the Young*, 13(5):451–460, 2003.

[15] K. H. Englmeier, G. Hellwig, J. Griebel, S. Delorme, M. Sieber, and G. Brix. Dynamic MR-mammography in virtual reality. *Studies in health technology and informatics*, 94:72–78, 2003.

[16] E. Dimitriadou, M. Barth, C. Windshberger, K. Hornik, and E. Moser. A quantitative comparison of funtional MRI. *Artificial Intelligence in*

*Medicine*, 31(1):57–71, 2004.

[17] C. Windishberger, M. Barth, C. Lamm, L. Shroeder, H. Bauer, R. Gur, and E. Moser. Fuzzy cluster analysis of high-field functional MRI data. *Artificial Intelligence in Medicine*, 29(3):203–223, 2003.

[18] D. Q. Zhang and S. C. Chen. A novel kernelize fuzzy C-means algorithm with application in medical image segmentation. *Artificial Intelligence in Medicine*, 32(1):37–50, 2004.

[19] P. Marzola, P. Farace, L. Calderan, C. Crescimanno, E. Lunati, E. Nicolato, D. Benati, A. Degrassi, A. Terron, J. Klapwijk, E. Pesenti, A. Sbarbati, and F. Osculati. In vivo mapping of fractional plasma volume (fpv) and endothelial transfer coefficient (kps) in solid tumors using a macromolecular contrast agent: correlation with histology and ultrastructure. *International Journal of Cancer*, 104(4):462–8, April 2003.

[20] P. Marzola, A. Degrassi, L. Calderan, P. Farace, C. Crescimanno, E. Nicolato, A. Giusti, E. Pesenti, A. Terron, A. Sbarbati, T. Abrams, L. Murray, and F. Osculati. In vivo assessment of antiangiogenic activity of SU6668 in an experimental colon carcinoma model. *Clinical Cancer Research*, 2(10):739–50, 2004.

[21] D. Comaniciu and P. Meer. Mean Shift: A Robust Approach Toward Feature Space Analysis. *IEEE Transactions Pattern Analysis and Machine Intelligence*, 24(5):603–619, 2002.

[22] D. A. Norman. *Thing that Make Us Smart*. Addison-Wesley, New York, USA, 1993.

[23] A. K. Jain, M. N. Murty, and P. J. Flynn. Data clustering: a review. *ACM Computing Survays*, 31(3):264–323, 1999.

[24] D. Pelleg and A. Moore. $X$-means: Extending $K$-means with efficient estimation of the number of clusters. In Pat Langley, editor, *Proceedings*

*of 17th International Conference on Machine Learning*, pages 727–734, San Francisco, USA, 2000. Morgan Kaufmann.

[25] D. Comaniciu. An algorithm for data-driven bandwidth selection. *IEEE Transactions Pattern Analysis and Machine Intelligence*, 25(2):281–288, 2003.

[26] T. Twellmann, O. Lichte, and T.W. Nattkemper. An adaptive tissue characterization network for model-freevisualization of dynamic contrast-enhanced magnetic resonance. *IEEE Transactions on Medical Imaging*, 24(10):1256–1266, 2005.

[27] T. W. Nattkemper, B. Arnrich, O. Lichte, W. Timm, A. Degenhard, L. Pointon, C. Hayes, and M. O. Leach. Evaluation of radiological features for breast tumor classification in clinical screening with machine learning methods. *Artificial Intelligence in Medicine*, 34(2):129–139, 2005.

[28] C. Varini, A. Degenhard, and T. W. Nattkemper. Visual exploratory analysis of DCE-MRI data in breast cancer by dimentional data reduction: a comparative study. *Biomedical Signal Processing and Control*, 1(1):56–63, 2006.

[29] Ogan M.D. Albumin labeled with Gd-DTPA. An intravascular contrast-enhancing agent for magnetic resonance blood pool imaging: preparation and characterization. *Investigative Radiology*, 12(23):961, 1988.

[30] H. Daldrup, D. M. Shames, M. Wendland, Y. Okuhata, T. M. Link, W. Rosenau, Y. Lu, and R. C. Brasch. Correlation of dynamic contrast-enhanced magnetic resonance imaging with histologic tumor grade: comparison of macromolecular and small-molecular contrast media. *Pediatric Radiology*, (28):67–78, 1998.

[31] K. Fukunaga. *Statistical Pattern Recognition*. Academic Press, New York, USA, 1990.

[32] D. Comaniciu, V. Ramesh, and P. Meer. The variable bandwidth mean shift and data-driven scale selection. In J. Little anb D. Lowe, editor, *IEEE International Conference on Computer Vision*, pages 438–445, Los Alamitos, USA, 2001. IEEE CS Press.

[33] S. Sheather and M. Jones. A reliable data-based bandwidth selection for kernel density estimation. *Journal of the Royal Statistical Society*, 53(3):683–690, 1991.

[34] M. P. Wand and M. C. Jones. *Kernel Smoothing*. Chapman and Hall, London, UK, 1995.